A MODEL FOR LARGE SCALE CONVECTIVE STORMS IN JUPITER

Ricardo Hueso[(1)], Agustín Sánchez-Lavega[(2)] and Tristan Guillot[(1)]

(1) Laboratoire Cassini, Observatoire de la Côte d'Azur, Nice, France.

(2) Departamento Física Aplicada I, Escuela de Ingenieros - Universidad Pais Vasco, Alda. Urquijo s/n. 48013 Bilbao, Spain.

Submitted to JGR: Planets

MANUSCRIPT PAGES: 32

TABLES: 2

FIGURES: 8

SHORT TITLE: Jovian Storms: Observations and Modeling

Send correspondence to:

Dr. Ricardo Hueso
Laboratoire Cassini
Observatoire de la Côte d'Azur
BP 4229
06304 Nice Cedex 04, France

E-mail: hueso@obs-nice.fr

Abstract:

Large-scale convective storms are a common phenomenon in Jupiter's atmosphere. They are apparent in ground-based and spacecraft images, and may strongly affect the dynamics of the global atmosphere as well as the energy transport in the meteorological layer. In this paper, we analyze the outburst of a large convective storm system (core ~ 5,000 km) in the South Equatorial Belt (SEB) that was observed at high spatial and temporal resolution by the Voyager 1 spacecraft in 1979. We use a 2D model to study the interaction between cloud material brought up by moist convection and the environmental wind. Aided by previous 3D models of jovian storms, we can draw several qualitative and quantitative conclusions. The evolution of this storm can be characterized by 3 phases: (1) Onset of the perturbation, well reproduced by the growth of a single-cell storm; (2) An expanding phase in which the number of convective cells increases to ~200, with updraft velocities limited to 50 m/sec; (3) A relatively sudden suppression of the convective activity leading to the disruption of large structures by the environmental wind. Furthermore, we interpret the observations of the inner bright core as a well-defined anticyclonic vortex, with darker cloud material preferentially left southwest of the system. Finally, we show that ~10^16 W are released by such a storm over its life cycle of 12 days and that the direct formation of a large scale anticyclonic vortex after the moist convective source has been removed is prevented by the environmental wind shear.

Key words: Jupiter, Atmosphere, Meteorology, Dynamics.

Index Terms: 5707 Atmospheres--structure and dynamics, 5739 Meteorology, 6220 Jupiter

1. Introduction

Moist convection in Jupiter is a powerful phenomenon suspected to play a key-role in the atmospheric dynamics (Ingersoll *et al.* 2000). Observations of convective storms at different scales (~ 1000 – 5000 km) have been very well documented from ground-based (see e.g. Sánchez-Lavega *et al.*, 1991; Sánchez-Lavega and Gómez, 1996; Sánchez-Lavega *et al.*, 1996) and spacecraft images (Smith *et al.* 1979, Banfield *et al.*, 1998; Gierasch *et al.*, 2000). Analysis of NIMS spectra obtained by the Galileo Orbiter showed a correlation between storm location and regions of high relative humidity (Roos-Serote *et al*. 2000). Lightning has also been observed by the Galileo Orbiter at specific latitudes (Little *et al.* 1999, Gierasch *et al.*, 2000). In some of these observations, the lightning occurs inside bright clouds that simultaneously display a strong convective activity. In particular, lightning has been shown to occur at several places in the same cloud system supporting the idea that the large-scale structure is composed of smaller convective cells. In particular, the South Equatorial Belt, located at planetographic latitudes ~ 10-20° S, is a common place for mid scale convective storms (<1000 km) westward of the Great Red Spot, and less frequent larger scale storms (~5000 km) that may evolve into planetary scale disturbances (SEBD). Radiative transfer analysis of the Galileo Orbiter's images performed in one of these mid-scale systems by Banfield *et al.* (1998) indicates that deep clouds were present at levels where only water can be in condensed form. In addition, Monte-Carlo simulations of the scattering of the light produced by lightning indicates a deep origin near the expected water cloud base (Dyudina *et al.* 2000). It is thus reasonable to assume that convective instability at the water cloud level is involved in such phenomenology. The abundance of water, the main ingredient for producing moist convection is not known. The in-situ measurements performed by the Galileo Probe were done in a locally dry area where the maximum abundance of water was only 0.2 times the solar value (Niemann *et al.*

1998). The bulk abundance of water in the planet (i.e. at deep levels) is significantly larger. Indeed the high location of the cloud tops retrieved by Banfield *et al.* (1998) suggests values of water abundance close to 2 times the solar value.

Several models for studying moist convection have been proposed for Jupiter. Stoker (1986) used a 1D model of moist convective entraining jets to estimate upper limits of the velocities and heights of the cloud tops for equatorial water and ammonia storms. In her model, only water was able to produce the kind of strong convection that sometimes occurs in the equatorial plumes and that were observed in detail by Voyager 1 and 2. Yair *et al.* (1992, 1995, 1998), used a 2D axisymmetric cumulus cloud model to investigate water convection. Their results suggested that water moist convection produce weaker storms with updrafts not powerful enough to reach the upper levels where storms are observed. Nakajima *et al.* (2000) used a 2D large-scale model driven by radiative cooling which produced frequent updrafts with velocities of the order of 20 m/s and no appreciable mixing between upper and deeper levels. Hueso and Sánchez-Lavega (2001) formulated a full 3D single-cell anelastic model for moist convection on Jupiter under a variety of chemical, dynamical and efficiency of precipitation conditions. They obtained that water storms are able to reach upper tropospheric levels (between 150 and 450 *mbar*) with intense updrafts of 40 to 150 *m*/*s* speed depending on environmental conditions and precipitation rates.

An important drawback inherent to single-cell models it that they do not reproduce mid-scale and large-scale storm observations. Storm systems that are observed in Jupiter are big structures that typically have sizes of a few thousand kilometers and develop over several days. However, detailed moist convective models explored to date are run for small regions of 100 km in size inside which one convective cell develops during a few hours. The single-cell models can not reproduce many of the observational aspects of storms in Jupiter due to computational limits.

In this work, we try to simulate and understand these large-scale events by linking our previous 3D single-cell models to a large-scale 2D horizontal "cluster model". The new model incorporates mass continuity, Coriolis and pressure force terms, and zonal wind shears. The cloud material is produced by every single-cell storm and then is distributed horizontally by the zonal winds. The model is explored in the context of the February 1979 SEB outburst imaged with high spatial and temporal resolution by the Voyager 1 spacecraft. The simulations generate information about the number of storms and average convective activity of the different cells needed to reproduce the observations.

In Section 2 we present a detailed analysis of such SEB outbursts which are modeled in the following sections. In Section 3 we explicit out the 2D numerical model and use the single-cell model to explore the time evolution of single-storms, calculate maximum sizes and investigate the development of anticyclonic vorticity in the system. We then present results of the cluster model when applied to the described Voyager storms. Section 4 is devoted to a discussion of energetic constraints obtained from the calculations and the observations. Section 5 discuss implications for vorticity generation and relationship with larger-scale eddies. Finally, Section 6 summarizes our conclusions from this work. The highly detailed Voyager 1 observations and part of the Voyager 2 observations were used to make movies that give more insight to the dynamics of these storms. Movies of the simulations are available as Windows avi files which can be downloaded from the web address: http://www.obs-nice.fr/hueso/ or obtained upon request to the authors.

2. The February 1979 SEB large-scale storm

The SEB outbursts or disturbances (SEBD) originate at planetographic latitudes 15-17º S in a region of almost null zonal wind (relative to System III) but with a cyclonic

large scale wind shear. These outburst have been extensively described and classified from historical and recent data by Sanchez-Lavega and Gomez (1996) and Sanchez-Lavega *et al.* (1996), so they will not be reviewed here. Instead, we concentrate on one particular episode that is very well documented in Voyager 1 high-resolution images and that will be used as a reference for our model simulations. Sánchez-Lavega and Gómez (1996) analyzed this storm and the cloud dispersion by zonal winds using a simple kinematic approach. Here we present a detailed dynamical study of the morphology of this storm system over its life cycle.

A movie of the Voyager images displaying the evolution of this system over 12 days was prepared by the authors. The movie has an average resolution of about 120 km/pixel with a time-span between images of 10 hours, and covers an area of 55° (longitude) x 20° (latitude) showing the dynamics of the whole area. Individual images attain much better resolution and allow measuring accurately the features sizes and drift rates. Figure 1 is a composite of snapshots of Voyager images showing different phases of the storm system. The whole cycle of storm development takes about 12 days, and this was the characteristic time for most of the convective features imaged by Voyager 1 and 2. About twelve of these events were observed by Voyager 2 four months later. They weakened after attaining maximum sizes of 4000-5000 km and in almost half of the cases led to a revival phase in which a new convective outburst appeared close to the previous storm. Morphologically about half of them were very similar to the storm described here. The other half presented significant changes in cloud shape and development probably due to their development on the turbulent wake of the Great Red Spot (GRS) at distances < 40º. The storm imaged by Voyager 1 presents exceptionally clear structures due to its development far away from other convective sites and to its large distance with respect to the GRS. Some caution must be taken in extrapolating the Voyagers observations to the usual dynamics of the SEB region. Although this kind of

storms have appeared at the SEB location several times in modern observations, they show a very high temporal variability in both number of storms and convective activity. Most frequently they only appear at the turbulent wake of the GRS, developing storms of ~2000 km which are highly sheared by the local turbulence. Voyager 1 and 2 captured the development of larger scale storms far away from the turbulent wake of the GRS. Note also that along extended temporal periods, the SEB has remained without traces of these large-convective storms that could have been seen even from ground-based observations (see Sanchez-Lavega and Gomez, 1996 for a review of the SEB behavior).

We used Voyager 1 Narrow Angle (NA) and Wide Angle (WA) images from FDS number 15960.26 (19 February 1979) to 16332.48 (3 Mars 1979) to measure the size of the central region where convection was developing. We could obtain images of the whole area studied almost every 10 hrs. Images where navigated and measured using the LAIA software package (developed by J. A. Cano from GEA, Spain) running under a conventional PC Windows computer. The LAIA software uses some VICAR based subroutines developed by C. Barnet at the New Mexico State University from the original Jet Propulsion Laboratory's Multimission Image Processing Laboratory VICAR (Jepsen *et al.* 1980). The pertinent navigation information was extracted from the Supplementary Experimental Data Record (SEDR) files. Details over navigating, correcting and measuring Voyager images can be found elsewhere (Barrey, 1984; Sada *et al.*, 1996).

The next step was the measurement of the storm size and growth rate. The central core is bright and presents high contrast with its environment over the whole development phase. Though it is irregular in shape, it is almost circular and its radius can be used to characterize its size. To measure the radius we developed an IDL (Interactive Data Language) program that counts the number of "bright" connected

pixels with an absolute threshold of luminosity of 80% of maximum brightness contour level. The bright core storm at each image was automatically identified and its area and radius measured. This is comparable to the procedure used by Hunt et al. (1982) in their measurements of the divergence of convective plumes on the North Equatorial Belt. We estimated the errors by taking into account pixel resolution and the variation of the core size that is obtained from slightly changing the chosen threshold to the limits that still permit to retrieve the core. 8.7 days after the first image, no more narrow-angle (NA) images of the central region where available and wide-angle (WA) images with lower resolution were used. Our automatic procedure failed to give well-defined values of area and radius. Measurements were then made visually making more difficult the estimation of errors. We verified that our IDL program and the visual measurements over the NA images provided nearly the same results.

Figure 2 shows our measurements of the horizontal growth of the SEB outburst core during analyzed 12-day period. The first 30 hours are dominated by a slow growth of a round bright cloud with no other structure. This feature tends to stabilize in size from time = 20 to 30 hours. We call this initial phase “Onset” (I in Figure 2). The first image of this phase is displayed at Figure 1A. Later, the system expands much more quickly to a larger size structure with the bright core and the development of the “tail” structure. This corresponds to Figure 1B and it is representative of the situation from days 2 to 7. At this time (II in Figure 2) the central core is of 5,000 km in diameter and the tail expands over 20,000 km. This is the “Mature” stage represented in Figure 1C. In the next hours, the region with bright clouds diminishes very quickly in size (III) although the tail continues to grow as it is drifted away by the jet westward winds. At the 10th day of its development the remaining small core seems to reactivate and grows again in size (IV) in a “Revival” phase of the convective storm. This phenomenon is imaged with a poor resolution at the WA images. At this time, a new convective core appears 5º

westward of the original core, as is apparent in Figure 1E and Figure 1F. Measurements in this plot correspond only to the initial core and do not take into account this new feature. Measurements of radial size over lower resolution Voyager 2 images of SEBD events display qualitatively the same results in growing rate, lifetime of the perturbances and revival phase of convective activity in nearly 50% of the cases. Analysis of this data was not included here because Voyager 2 images of these storms had typically four times lower resolution than that of Voyager 1. This lower quality prevented us to study the first stage of onset of the storm in any of the Voyager 2 storms.

3. Mass continuity numerical simulations of storm dynamics

3.1. Model Design

Full domain and detailed high-resolution numerical calculations of these convective structures are not feasible due to the large area involved. Instead, coupling of results from a detailed 3D model describing a single convective event (Hueso and Sánchez-Lavega, 2001) and a global 2D mass continuity "multi-cell model" is used to give insight over the possible dynamic scenarios for the SEBD events.

A 2D model that incorporates mass continuity, Coriolis forces and the interaction with the environmental winds is presented. The model solves in time the dynamic equations over a layer of fixed potential temperature where the mean motions are supposed to be fully horizontal.

We solve the following equations:

$$\frac{Du}{Dt} = +fv - \frac{1}{\rho}\frac{\partial \pi}{\partial x}, \qquad (1)$$

$$\frac{Dv}{Dt} = -fu - \frac{1}{\rho}\frac{\partial \pi}{\partial y}, \qquad (2)$$

where D/Dt is the total derivative, f is the Coriolis parameter defined by $f = 2\Omega \, \mathrm{Sin}(\varphi)$, being φ the planetographic latitude, Ω the angular rotation velocity of the planet, π is the pressure, and ρ is the density at the pressure level where horizontal cloud motions are supposed to occur (P ~ 600 mb, $\rho \sim 1.3\ 10^{-4}$ g/cm^3).

The model is initialized using the zonal wind profile measured by Limaye (1986). To make the large-scale horizontal winds stable under the Coriolis forces a Coriolis related pressure field π_c is defined that verifies $\partial \pi_c / \partial x = -fv\rho$, so that equations (1) and (2) are fulfilled for the defined wind profile. The storm is introduced in the model as a divergent source at the central position of the grid with characteristic radius R_0 and an outward expanding horizontal velocity V_r. The convective region also possesses a perturbation pressure field π_s arising from the dynamics in the inner region.

Values for R_0, V_r and π_s are obtained from our accurate 3D simulations of moist convection. We retrieve the velocity field (vertical and horizontal) and the cell size at the ammonia level cloud for different conditions (see e.g. Tables 1 and 2 in Hueso and Sánchez-Lavega, 2001). These data are used to estimate relations between vertical ascending velocities and horizontal outflows at the ammonia cloud deck and also the pressure perturbations induced at the upper level (pressure range from P_1 ~ 650 to P_2 ~ 450). In the 3D simulations we found that R_0 can not be substantially larger than 25 km. The physical reason is that at those values mass continuity can not be preserved in the updraft if the energy is provided at the 5-6 bar levels. Simulated updrafts tend to break in smaller ones when they grow to sizes larger than that. The associated perturbation

pressure field, π_s, can be described by means of an empirical relation as a function of the expanding velocity V_r,

$$\pi_s = \pi_0 (V_r/50) + \pi_1 (V_r/50)^2, \qquad \text{for } r < R_0, \tag{3a}$$

$$\pi_s = \left[\pi_0 (V_r/50) + \pi_1 (V_r/50)^2\right] \frac{R_0}{r}, \qquad \text{for } r > R_0. \tag{3b}$$

where π_0 = 3 mbar, π_1 = 1.3 mbar and V_r is given in m/s. Radial velocities V_r correlate with upward velocities in the storm and depend on atmospheric condition so that different values of V_r must be explored.

Outside the central region, vertical motions are assumed to be small enough to allow for two-dimensional mass continuity:

$$Div\, \mathbf{V} = \frac{\partial u}{\partial x} + \frac{\partial v}{\partial y} = 0. \tag{4}$$

A passive tracer that represents the cloud material produced by the storm is introduced in the model so that it has a constant value inside the storm core. Outside this region it is carried by the wind following the advective equation,

$$\frac{Dq}{Dt} = 0. \tag{5}$$

The model is integrated in time using a non-staggered two-dimensional grid. The numerical procedures used to solve the model equations are 2D versions of the methods described in detail in Hueso and Sánchez-Lavega (2001). The method of dimensional

separation is used to separate advective terms from source terms. Advection terms are treated using a four points upwind scheme while time integration is done according to a Crank-Nicholson implicit scheme, source terms are forward integrated in time (Fletcher, 1997). In particular, our numerical procedure includes mass continuity by minimizing locally in an iterative way the value of *Div* **V** in Eq. (4) at every point outside of the storm core. Inner boundary conditions that depend on storm characteristics, R_0 and V_r, are placed in the grid points inside the storm core. Boundary conditions at grid limits are soft so that material that comes into the grid by convection can go out of the numerical domain through the grid walls.

The model is used in two different ways. First, we perform simulations of single-storm cells when only one region of divergence is considered. This provides information over the "Onset" phase of the storm. Later, we allow the model to treat simultaneously various convective cores simulating a cluster of updrafts, providing information over the number of storms in the expanding and "Mature" phases of the SEBD cycle.

3.2. Single-storm calculations

We performed different calculations of a continuously active convective core at latitude 16ºS in a grid of 1000x500 points and resolution of 5 km per grid point. Our calculations were run for values of V_r of 15, 30, 50 and 100 m/s spanning a total time of 120 hrs. Some others simulations were performed with different grid resolutions to check model's consistency. We found that a resolution of 10 km per grid point is needed to obtain consistent results. This is reasonable since our source has dimensions of 50-km diameter. The role of the π_s field associated with the updraft is very small or even negligible for a single core storm. However, its importance is larger in the case of

ensembles of convective updrafts, where the cumulative effect of every single core may become non-negligible.

Figure 3 shows a conceptual scheme of the 2D-model together with time-steps of the cloud field evolution for the case V_r =30 m/s. The qualitative evolution of a single-storm was very similar in all the simulations. In all the cases studied, the storm evolves very quickly during the first 5-10 hours following a radial expanding motion with almost a constant growing rate (Figure 3A). At this time, Coriolis terms have developed anticyclonic vorticity along the outer part of the cloud. Vorticity tends to confine the motions making further expansion more difficult (Figure 3B). The system continues to grow at a lower rate interacting also with the cyclonic wind shear. The zonal wind drives away from the source part of the outer cloud material (Figure 3C), and deforms the anticyclone in formation. Because the zonal cyclonic wind opposes strongly the anticyclonic motions of the storm, the interaction develops small cyclonic and anticyclonic eddies that propagate with the wind in a two tail-like structures (Figure 3D). The number of such eddies depends strongly on the particular value of V_r, with increasing values of this parameter producing more turbulence. However, the size of the eddies apparently does not depend on this parameter, and they remain quite stable while being carried out by the wind. However, this is not the case for the large anticyclone. If the convective source is removed, the central anticyclone eventually fails to maintain itself as a stable structure and is broken appart very quickly in a turbulent pattern by the environmental wind. We will come back to this point in Section 5.

In Figure 4 we compare the single-cell model radial size evolution and the observations of the SEBD during the first 3 days of storm development. The simulations behave qualitatively in the same way for the cases, with larger sizes reached for larger values of V_r . It is interesting to note that the case V_r = 30 m/s reproduces the initial evolution of the real storm. Larger velocities produce storms that grow in time much

faster than what the Voyager observations show, and weaker storms with radial expanding motions < 15 m/s would grow too slowly creating only a small size feature. It is apparent from a comparison between the model results and the measurements over the SEB outburst, that a single cell storm with V_r ~30 m/s can explain the size of the system only during the first 20-30 hours. This corresponds to updrafts with W ~ 40 m/s, typical of the three-dimensional simulations in Hueso and Sánchez-Lavega (2001). Table 1 summarizes the results obtained for the different cases and phases of storm-vortex development. It also presents what are the most likely updraft velocities and cloud tops reached for each 2D simulation according to 3D simulations.

In conclusion, no single storm, even considering unreasonable large values for V_r would be able to reach the large size of the "Mature" SEBD. Different updrafts must operate at the same time and this point is addressed in the next section.

3.3. A cluster of cells to simulate the SEB outburst

A successful model for a large-scale storm system can be constructed by placing not one, but various convective cells. We will consider that all the updrafts have the same characteristics, R_0 and V_r, and that they are spaced at equal intervals ΔC in the grid. Although this represents a simplification of the real situation, the model provides information over the average behavior of the different elements.

We activate the convective cells sequentially at different times in order to fit the size and general behavior of the observations of the SEBD event. We begin the simulations with one single-cloud element for V_r = 30 m/s, a value that approximately fits the observations for the first 30 hours. Nearby convective cores are then activated when the area of the simulated storm is smaller than 90 % of that fitted by a polynomial to the data. The real SEBD events do not grow symmetrically from the original source, but northwards and westwards as it can be seen in Figure 1. We include this effect in our

simulations activating the convective cores only at the northwest quadrant of the grid. We activated each core following their distances to the initial onset and activating cores located at the same distance from the origin from west to east.

The mechanism that triggers the sequential convective cells is not studied here. In classical simulations of storm systems in the Earth's atmosphere, the gust front that forms when downdrafts reach the ground is the most important factor controlling the regeneration, propagation and development of new cells (Lin, Y.L. *et al.* 1998, 2001). In a planet without a surface a gust front is not easy to develop and downdrafts can reach very deep atmospheric levels without altering its environment. We anticipate that large-scale moisture transport by advection and precipitation could play an essential role in the giant planets atmosphere. At this time, however, we can only use the "cluster" model to infer the number and general characteristics of convective cells active at different times of the SEBD evolution.

Several low-resolution 2D-simulations (Δx = 20 km) were performed by varying the parameters of the model. A nominal value of $\Delta C \sim 250$ km was found to provide homogeneous coverage of clouds in the SEBD region at all times while avoiding an unreasonably high production of turbulence and eddies. The most interesting "cluster" simulations were those studied in domains of 8,000 x 8,000 km and high-resolution grids with $\Delta x = 10$ *km*, and results are given in Table 2. The table shows the parameters defining the cluster simulations as well as the number of storms required to fit the size of the SEBD at time = 5 days and the corresponding maximal tangential velocities at the cluster periphery. Simulations for longer times were not performed since the storm system grows to sizes larger than our computational domain. The number of active single-cells needed to match the size of the SEB outburst core is an important issue, since it relates directly to the amount of energy given to the atmosphere. This point will be discussed in next section.

A common characteristic in all the simulations is the anticyclonic vorticity that develops in the periphery of the system. Global vorticity appears because of the anticyclonic rotation at every single convective element in the periphery of the system. The case named “nominal” (Nom in Table 2) produced the best agreement between model and the observations. Cases V1 and V2 were performed to test model behavior when weaker (V1, V_r = 15 m/s) and stronger (V2, V_r = 40 m/s) cell elements are used. In the first case individual cells did not grow to cover the whole size of the SEBD core providing strong differences with the observations at all times. The second case fits quite well the observations for times longer than 2 days but produced very different structures at lower times. Cases D1 and D2 were used to test model behavior when varying the average distance between storm elements. If cell elements are too close (D1, ΔC = 100 km) they have trouble to distribute all the produced cloud material and quickly forming turbulent eddies expel the material between cells. Moreover, they can not fully grow since they feel so strongly the presence of nearby cells and the whole system acquires a patchy aspect that is not observed. If on the other hand, the cell elements are too far away from each other (D2, ΔC = 300 km), the system also presents a patchy global structure but not outward motions between cells appears. For longer times, however, cloud diffusion between adjacent cells permits to homogeneously cover the SEBD core region providing a good fit to the observations.

The nominal case yields a reasonable fit to the observations for all times studied. Figure 5 presents snapshots of the evolution of the cloud field for this scenario (V_r =30 m/s, R_0=25 km and ΔC=250 km). Bright clouds are produced at every active convective core and can be traced in each image. The “gray clouds” correspond to material initially at a radius of 2,500 km from the onset source and they are introduced to reproduce the southern tail-like structure evident in the observations. The initial onset is dominated by the single-cell storm that we studied in Section 3.1. Later, new cores are activated

covering efficiently the central region and fitting the size of the observations. The rotation of every core in the cluster produces an average anticyclonic rotation at the periphery of the system with tangential velocities V_t ~ 100 m/s. The average circulating pattern can also be identified in Figure 5 and it is very conspicuous in the movies of the simulation. As in the case of single-cell storms the wind shear produces eddies with vorticity of both signs. Anticyclonic motions appear on Voyager 1 images around the time the storm develops its maximum activity (C in Figure 1). Although no individual cloud tracers could be found to accurately measure wind velocities, detailed analysis of cloud morphology and motions inferred in the movie strongly suggest anticyclonic circulation. Gierasch et al. (2000) analyzed Galileo Orbiter images of an elongated 4,000 km storm in the SEB at the turbulent wake of the GRS. They obtained a map of the motions at the cloud tops. These were apparently dominated by the turbulent wake of the GRS and by the interaction with a nearby storm. No significant anticyclonic motions were found inside the storm, although significant vorticity of both signs was present in its neighboring.

Figure 6 shows the evolution of the radial size of this "cluster" simulation compared to the observations as well as the number of the necessary "active" cells. The number of active storm cores follows a parabolic fit that predicts a maximum number of updrafts of ~ 180-200 when the maximum size of the SEBD is reached.

4. Energetic constraints

Energy deposition by moist convection in the upper atmosphere of Jupiter has been recently examined following the analysis of mid-scale storms in the Galileo spacecraft SSI images (Banfield *et al.*, 1998; Gierasch *et al.* 2000, Ingersoll *et al.* 2000). The Galileo Orbiter took images of a convective feature on the SEB with a size of 1,000 *km*.

According to Gierasch *et al.* (2000), storms of this type could provide to the atmosphere large amounts of thermal power (~ 5 x 10^{15} W) coming from the release of latent heat of water. These authors extended their analysis to the whole planet using lightning observations performed by the Galileo spacecraft (Little *et al.* 1999) as a measure of global moist convective activity in the planet. They concluded that the total amount of thermal energy released by moist convection averaged over the planet could be as high as 3.3 W m^{-2}. As Jupiter's internal heat flux averaged over the planet is 5.7 W m^{-2} moist convection could play an essential role in the atmospheric dynamics. These ideas were further developed by Ingersoll *et al.* (2000). They argued that eddies, the large anticyclone ovals, and ultimately the jets in Jupiter's atmosphere, could receive most of their energy from moist convection, which should be responsible of a large part of the atmospheric dynamics.

Banfield *et al.* (1998) presented a similar analysis for the Voyager 2 images of the SEB storms, obtaining a total power of 1.4 x 10^{16} W for these convective events. We will use here the method they considered for their estimations but using our improved measurements of the event presented in Section 2. This allows us to consider the power released at the different stages of storm development. We also present a similar analysis for the different simulations described in Section 3.

Assuming that the flow divergence occurs mainly over one scale-height from levels P_0 ~ 1 bar to P_{top} ~ 400 mbar as suggested by our model, we can calculate the total heat content and the power released by the storm system as

$$Q = A\frac{P_0 C_p \Delta T}{g}, \qquad (7)$$

$$P = \frac{dQ}{dt} = \frac{P_0 C_p \Delta T}{g} \frac{dA}{dt}, \quad (8)$$

where Q is the total heat content of the storm, A is its area, C_p =1.3 x 10^4 J Kg^{-1} K^{-1}, g = 23 m s^{-2} and P is the power released. The cloud height of 400 mbar measured over the Galileo images provided a value of ΔT = 5 K which, according to modeling of moist convection (Hueso and Sánchez-Lavega, 2001) corresponds to a deep water abundance ~ 2 times the solar value.

Figure 7 presents the evolution of the power released in the atmosphere by the studied SEBD event. The solid thick line corresponds to the power calculated from the measurements of the storm area evolution using a water abundance 2 times solar. The dashed region marks the range of possible values of power released taking into account our estimation of errors. It corresponds to a range of water abundances from 1 to 3 times solar and has as upper and lower limits for the storm size those plotted in Figure 2. The estimations from Banfield *et al.* (1998) and Gierasch *et al.* (2000) appear as a diamond and a circle respectively. Interestingly, the power released by the storm system remains constant over a large period of time (stage II in Figures 2 and 7) that, according to our interpretation, corresponds to the phase where different upward cells are activated.

A similar analysis can be performed over the simulations, including in addition the amount of kinetic energy deposited in the atmosphere by the outflows. This is given as

$$P_{kin} = \frac{dM}{dt} \frac{V_r^2}{2}, \quad (9)$$

where M is the total mass involved in the outflow and (9) is evaluated over a cylinder of radius R_0 with outflow velocities V_r. The same considerations that were used in (7) can

be established here: outward motions take place over one scale height with its base located at P_0 ~1 bar. Then

$$P_{kin} = \pi \frac{R_0 P_0}{g} \frac{V_r^3}{2} . \quad (10)$$

For the simulated single-cell storms, using Eq. (8) and assuming ΔT = 5 K, we get maximum values of the released thermal power = 4.2×10^{14}, 1.0×10^{15}, 1.6×10^{15} and 4.7×10^{15} W for storms with 15, 30, 50 and 100 m/s radial velocities respectively. Kinetic energy is however a constant in these simulations. From Eq. (10) we obtain 5.8×10^{11}, 4.6×10^{12}, 2.1×10^{13}, and 1.7×10^{14}W for the above cases. For all of the simulations, the thermal energy component is always significantly higher than the kinetic energy. The ratio between both types of energy provides a measure of the efficiency of conversion from thermal to kinetic energy. The corresponding ratios between kinetic and thermal power are 0.2, 0.5, 1.5, and 5 % for the above mentioned cases.

The power released by our cluster-system of storms can also be analyzed from the simulations. Both thermal (dashed line) and kinetic (dotted line) powers produced by the simulated storm cluster are plotted in Figure 7. The ratio between kinetic and thermal energy is always close to 1 %, which is a reasonable value for atmospheric dynamics. This means that most of the energy transported is in the form of thermal energy and may be redistributed in the atmosphere over long periods of time while kinetic energy brought quickly, comes in a much lower quantity.

For the whole SEBD event of our nominal cluster simulation, the average thermal released power is ~ 1.4×10^{16} W while the kinetic released power is 3.9×10^{14} W. Full transmission of the internal heat source of Jupiter by moist convection requires that

the amount of active storms needed at any time would occupy a small fraction of the total surface of the planet. We estimate this to be between 0.1% (for the smallest single storms that we have examined) to 4% (for the largest events like the SEBD). Results for the cluster model are far from being additive with respect to the single-cells which compose it. A cluster of *N* nearby convective cells provides much less energy than the same number *N* of dispersed cells, since in the first case the interaction between the cells impedes its full development. Nearby updrafts provide close-in divergence sources that inhibit the expansion of the uplifted clouds. In this sense, small-scale moist convection operating simultaneously at several places, would be a better candidate for transporting the internal heat source of the planet that single cluster-like large-scale storms, as those observed in the SEB.

5. Consequences for vortices development

Although the SEB is a relatively low latitude region of Jupiter (16ºS), Coriolis forces are not negligible for storm systems that endure several days as those that we have studied. In the previous sections we have shown that Coriolis forces play an essential role in the rotation of single cells, producing a peripheral anticyclonic vorticity of the global system. However, the anticyclonic circulation is located in a region of average cyclonic vorticity as determined by the environment zonal wind shear. This counter-rotation produces tail-like structures where the high wind shear creates a varying number of small eddies with both kinds of vorticity. The wind shear at the location of the storm onset is only symmetric at scales ~ 500 km (See Figure 1A). The tail-like structures that develop later move at different velocities with a fast southern branch that moves eastward at ~ 40 m/s and a northern branch that moves westward at

28 m/s. Both features are passively carried by the wind while they transport the small eddies which remain stable over the whole time of our simulations.

The central anticyclone represents the most important contribution to vorticity. However, it is not stable in time. For all of the simulations, the central storm-vortex system loses its coherence whenever the central divergence source is not present. If we make the convective activity decrease after a certain time, the ambient cyclonic wind shear has no difficulties in breaking the large anticyclonic region. What remains after a few tens of hours is a pattern of turbulence continuously dispersed by the wind, although some stable regions of vorticity of both signs with typical sizes of 50 - 100 km could survive in the tail region.

From our 2D simulations we must conclude that moist convection is not able to generate large-scale stable eddies in just one step but, perhaps, if it does, only through more complicated processes not evident from our model. Although moist convection is a powerful source of energy, the step between the storm release of energy and the generation of large-scale eddies is not evident. It seems more plausible that these eddies obtain their energy from mixing of smaller-scale vortices than directly from the convective events.

6. Conclusions

In this paper we have studied large-scale convective storms in Jupiter. We have presented a detailed analysis of a typical large-scale convective event in Jupiter and performed two-dimensional modeling of this structure. This 2D-model act as a link with the more accurate 3D treatments of moist convection for small regions presented previously (Hueso and Sánchez-Lavega, 2001).

For the evolution of a large-scale SEB outburst, a scenario with several convective cells ("storm cluster") operating simultaneously, is able to reproduce qualitatively the visual aspect and basic properties of the event as revealed by the observations. We presently do not know which mechanism is able to trigger the development of the sequence of cells in the cluster, but downdrafts and gust fronts at the water condensation level are probably part of it. The best model to explain the SEBD outbursts includes a phase of single storm development for ~ 20 hrs with updrafts of ~ 40 m/s and outwards motions of ~ 30 m/s. From the 3D modeling we know that this kind of moist convective storms may form in the atmosphere of Jupiter under reasonable values of atmospheric conditions. For the storm to develop the size and characteristics of the SEBD, a second phase of quick activation of new updrafts with similar characteristics is needed. The cluster simulation that best agrees with the observations produces a maximum number of updrafts on the order of ~ 200 cells. The tail-like structures are well reproduced by environment material that is carried out by the wind without being dynamically active. In addition, interaction between the bright clouds, carried to high levels by moist convection, and surrounding clouds, not uplifted by the storm, may help to create the initial tail structures. Unfortunately, this is a point that the 2D models presented here can not address. Figure 8 is a schematic conceptual view of the storm system as we have described it.

The whole storm system analyzed here can be very energetic, releasing a power of 10^{16} W of thermal energy and 10^{14} W of kinetic energy. Energetic analysis of these storms is consistent with a large transport of internal heat by moist convection. However, it is not evident how this power can be transferred to the ambient winds. Most of the energy is released as a thermal component with a minor component of kinetic energy. As showed by Sanchez-Lavega *et al.* (1996) no changes on the mean zonal winds were noted during the evolution of a powerful SEBD event that occurred in 1993.

The global contribution to the dynamics from moist convection is an interesting subject but needs more data concerning the distribution and amount of convective activity over the planet. On the other hand, anticyclonic vorticity is easily generated in the system. The main anticyclonic eddies are quickly destroyed by the cyclonic environment winds when no convection is considered, so there is not a direct transition from a convective wet storm to a mid-scale vortex. Small-scale eddies (50-100 km) that move with the wind are able to survive for longer periods without much dissipation.

The subject of moist convection on the giant planets has benefited of large interest in view of the observations from the Galileo mission to Jupiter (1995 to the present). Unfortunately, the Galileo observations failed to provide large-temporal coverage of observed events because of problems with the main antenna. In October-December 2000 the Cassini-Huygens mission to Saturn performed a flyby to Jupiter obtaining detailed observations of the whole atmosphere of the planet over 3 months of time but with a lower spatial resolution. Analysis of this data should provide more accurate constraints to the convective activity of the planet which would yield important hints for models of atmospheric dynamics.

Acknowledgements

We thank J. A. Cano of the Grup d'Estudis Astronòmics (GEA) for their effort in adapting the VICAR codes to the software package LAIA. This work has been supported by *Programme National de Planetologie* (French team) and by the Spanish MCYT research project PNAYA2000-0932 (A. Sanchez-Lavega). R. Hueso acknowledges a Post-doctoral fellowship from Gobierno Vasco. Calculations were performed at the Suppe PC cluster at the Observatoire de la Côte d'Azur. We also acknowledge the National Space Science Data Center (NSSDC) through the World Data

Center A for Rockets and Satellites for providing the Voyager images. The Voyager Experiment Team Leader was Dr. Bradford A. Smith.

REFERENCES

Banfield, D., P. J. Gierasch, M. Bell, E. Ustinov, A. P. Ingersoll, A. R. Vasavada, R. A. West and M. J. S. Belton. 1998. Jupiter's Cloud Structure from Galileo Imaging Data. *Icarus*, **135**, 230-250.

Barrey, R. F. T. 1984. *A User's Guide to Voyager Image Processing*. Imperial College, London.

Dyudina, U. A., A. P. Ingersoll and the Galileo SSI Team, Modeling of Jovian Lightning Imaged by Galileo SSI Camera, paper presented at the 32nd Meeting of the Division of Planetary Sciences, Pasadena, USA, 2000.

Fletcher, C. A. J. 1997. *Computational Techniques for Fluid Dynamics, Vol 1, Fundamental and General Techniques*. Springer-Verlag, New York.

Gierasch, P. J., A. P. Ingersoll, D. Banfield, S. P. Ewald, P. Helfenstein, A. Simon-Miller, A. Vasavada, H. H. Breneman, D. A. Senske and the Galileo Imaging Team. 2000. Observations of moist convection in Jupiter's atmosphere. *Nature*, 403, 628-630.

Hueso, R., and A. Sánchez-Lavega. 2001. A Three-Dimensional model of moist convection for the Giant Planets: The Jupiter case. *Icarus* **151**, 257-274.

Hunt, G. E., J. P. Müller and P. Gee. 1982. Convective growth rates of equatorial features in the jovian atmosphere. *Nature*, **295**, 491-494.

Ingersoll, A. P., P. J. Gierasch, D. Banfield, A. R. Vasavada and the Galileo Imaging Team, 2000. Moist convection as an energy source for the large-scale motions in Jupiter's atmosphere. *Nature*, **403**, 630-632.

Jepsen, P. L., J. A., Moser, G. M. Yagi, C. C. Avis, J. J. Lorre, and G. W. Garneau 1980. Voyager image processing and the Image Processing Laboratory. *J. Br. Interplanet. Soc.* **33**, 315-322.

Little, B., C. D. Anger, A. P. Ingersoll, A. R. Vasavada, D. A. Senske, H. H. Breneman, W. J. Borucki and The Galileo SSI Team, 1999. Galileo Images of Lightning on Jupiter. *Icarus*, **142**, 306-323.

Limaye, S. S., 1986. Jupiter: New estimates of the mean zonal flow at the cloud level. *Icarus* **65**, 335-352.

Lin, Y. L., R. L. Deal, and Mark S. Kulie. 1998. Two-Dimensional Multicell Storm, *J. Atm. Sci.* **55**, 1867–1886.

Lin, Y. L., and L. E. Joyce, 2001. A further study of the mechanisms of cell regeneration, propagation, and development within two-dimensional multicell storms. *J. Atm. Sci.* **58**, 2,957–2,988.

Nakajima, K., S. I. Takehiro, M. Ishiwatari, Y. Y. Hayashi, 2000. Numerical modeling of Jupiter's moist convection layer. *Geophys. Res. Lett*. **27**, 3,129-3,132.

Niemann, H. B., S. K. Atreya, G. N. Carignan, T. M. Donahue, J. A. Haberman, D. N. Harpold, R. E. Hartle, D. M. Hunten, W. T. Kasprzak, R. Mahaffy, T. C. Owen, and S. H. Way, 1998. The composition of the jovian atmosphere as determined by the Galileo probe mass spectrometer. *J. Geophys. Res.* **103**, 22831-22845.

Roos-Serote, M., A. R. Vasavada, L. Kamp, P. Drossart, P. Irwin, C. Nixon and R. W. Carlson, 2000. Proximate humid and dry regions in Jupiter's atmosphere indicate complex local meteorology. *Nature*, **405**, 158-160.

Sada, P. V., R. F. Beebe, and B. J. Conrath 1996. Comparation of the structure and dynamics of Jupiter's Great Red Spot between the Voyager 1 and 2 encounters. *Icarus* **119**, 311-315.

Sánchez-Lavega, A., I. Miyazaki, D. Parker, P. Laques, and J. Lechacheux, 1991. A disturbance in Jupiter's high-speed north temperate jet during 1990. *Icarus* **94**, 92-97.

Sánchez-Lavega A. and J. M. Gómez, 1996. The South Equatorial Belt of Jupiter, I: Its Life Cycle. *Icarus* **121**, 1-17.

Sánchez-Lavaga, A., J. M. Gómez, J. Lecacheux, F. Colas, I. Miyazaki, D. Parker and J. Guarro, 1996. The South Equatorial Belt of Jupiter, II: The Onset and Development of the 1993 Disturbance. *Icarus*, **121**, 18-29.

Smith, B. A., L. A. Soderblom, T. V. Johnson, A. P. Ingersoll, S. A. Collins, E. M. Shoemaker, G. E. Hunt, H. Masursky, M. H. Carr, M. E. Davies, A. F. Cook, J. M. Boyce, T. Owen, G. E. Danielson, C. Sagan, R. F. Beebe, J. Veverka, J. F. McCauley,

R. G. Strom, D. Morrison, G. A. Briggs, V. E. Suomi, 1979. The Jupiter system through the eyes of Voyager 1. *Science*, **204**, 951-972.

Stoker, C. R., 1986. Moist Convection: A Mechanism for Producing the Vertical Structure of the Jovian Equatorial Plumes. *Icarus* **67**, 106-125.

Yair, Y., Z. Levin, and S. Tzivion. 1992. Water-Cumulus in Jupiter's Atmosphere: Numerical Experiments with and Axisymmetric Cloud Model. *Icarus*, **98**, 72-81.

Yair, Y., Z. Levin, and S. Tzivion. 1995. Microphysical Processes and Dynamics of a Jovian Thundercloud. *Icarus*, **114**, 278-299.

Yair, Y., Z. Levin, and S. Tzivion. 1998. Model interpretation of Jovian lightning activity and the Galileo Probe results. *J. Geophys. Res.*, **103**, 14,157-14,166.

FIGURE CAPTIONS

Figure 1: Cylindrical projections of the time evolution of the SEBD event imaged by Voyager 1 in February 1979. Images were selected to illustrate different phases in the development of this storm. The area represented occupies 55º in longitude x 20º in latitude, horizontal ticks are every 5º and vertical every 2º. Central latitude is 16º S. The first panel indicates the wind profile measured by Limaye (1986). All times are relative to the first image. (A) "Normal": FDS No. 15960.26, 19 February 1979, time = 0 *hrs*; arrow points to storm onset location. (B) "Onset": FDS No 16046.59, time = 2,9 days; the developing convective system is characterized by a bright nucleus and a fainter tail of dispersed material. (C) "Mature": FDS No 16171.58, time = 7.1 days. Here the core attains its maximum size (5,000 *km* in diameter) and the dispersed material shows a lot of structure spanning 20,000 km long. (D) "Decaying": FDS No 16207.36, time = 8.2 days. This high-resolution image of the storm core shows structure and smaller-scale convective activity in the southeastern part. (E) "Revival": FDS No 16307.33, time = 11.7 days. There is a revival of activity in the location of the initial storm, and an outburst of a new convective feature 5° westward of it. (F) FDS No16332.48, time = 12.5 days. This wide-angle image of both storms shows them connected by a tail feature coming from the first outburst. All the images are displayed here with the same resolution except for image (D) that is displayed with a higher resolution. Arrows in D, E and F mark the location of active convective regions.

Figure 2: Measurements of the radial size of the SEB convective core as a function of time. Filled circles correspond to measurements over high resolution NA images, empty circles to measurements over approximately four times less resolution WA images were

contrast between core and nearby structures was also lower. The dashed lines are a polynomial fit to the data for the different evolution stages indicated as I (Onset), II (Rapid growth to a Mature stage), III (Decaying) and IV (Revival).

Figure 3: Scheme of a typical single-cell storm simulation evolution (left) and model behavior for the case V_r = 30 *m*/sec (right) where clouds are represented by a passive tracer. The domain represented on the right panels is 3,200 x 1,600 *km*. (A) Time = 10 *hrs*. The region is dominated by outward motions with radial velocity V_r. The central divergent source of 25-*km* radial size is marked as a grey central dot on the left. (B) Time = 30 hrs. Outwards radial velocities expand the region covered by the passive tracer and rotation driven by Coriolis forces is now very strong developing an anticyclonic circulation with speed 25 *m*/*sec*. (C) Time = 80 hrs. The system grows to a size large enough to feel the environment wind shear and deforms accordingly. (D) Time = 200 hrs. The system is completely developed and has a forming main anticyclone vortex, and series of eddies developing in the north and south branches of the storm that are drifted away by the wind. Although most of the structure here resembles that of the observations, the model storm is more than 5 times smaller.

Figure 4: Onset phase of the storm. Black dots refers to measurements over the Voyager 1 images, lines represent the radial size of a simulated single-storm cell for different values of the outwards radial velocity. Dotted line, continuous, dashed and dot-dashed lines are for 15, 30, 50 and 100 m/sec, respectively.

Figure 5: Snapshots of cluster simulation evolution. The whole domain of 900 x 900 points (9.000 x 9000 km) is displayed here for selected times (= 30, 50, 70, 100 and 120 hrs after onset) and number of active storms (N). Bright material comes only from

active convective cores and gray material is used to plot the evolution of the cloud originally at a radius of 2.5000 km from the initial onset spot. The last panel shows, at the same scale and time evolution the Voyager 1 storm together with the corresponding final simulation.

Figure 6: Cluster model results for the nominal case. A) Measured radial size of the storm (dots) and retrieved radius evolution for the nominal cluster simulation (solid line). B) Number of storms at every time step needed in the nominal simulation to fit the radial data. The fit tentatively predicts a maximum number of ~200 single cells at the time of maximum size.

Figure 7: Power released by the SEBD outburst aimulation at different stages: (I) Onset, (II) Development, and (III) Decreasing activity. The solid line corresponds to our measurements of radial size with assuming 2 times solar water composition. The dashed region plots the possible range of values for the power release taking into account uncertainties in the storm size and water abundance (range 1-3 times solar composition). Estimations by Banfield *et al.* (1998) of a similar SEBD event (diamond) and by Gierasch *et al.* (2000) for a smaller convective event (empty circle) are also indicated. The dashed and dotted lines represent respectively the thermal and kinetic power released by the nominal cluster simulation.

Figure 8: Conceptual schematic view of the SEBD storm system. Bright clouds on the observations correspond to cloud tops whose coherence is maintained by Coriolis forces. The central ascending region may be composed of several different convective updrafts. In this view, gray darker clouds in the tail-like structure would correspond to

environmental, deeper cloud material that does not experience significant divergence and that is just carried by the wind. The cyclonic wind profile is more intense in the southern branch of the storm developing a stronger tail in this region than in the northern branch. Global transport of moisture by precipitation may be related to the mechanism that produces new convective cells East and North of the original site (dashed arrow).

Table 1

Summary of single-cell model simulations

Grid characteristics	**Storm parameters**		**Correlation with 3D simulations**			**2D Results**	
1,000 x 500 points	V_r (*m/sec*)	R_0 (*km*)	W (*m/sec*)	P_{top} (*mb*)		Max Size	$V_{\text{tangential}}$
Resolution: 5 *km*	15	25	30	600	(*)	240 *km*	20 *m/sec*
Central latitude:	30	"	40	450	(†)	330 *km*	30 *m/sec*
16ºS	50	"	60	320	-	425 *km*	40 *m/sec*
	100	"	130	150	(§)	600 *km*	65 *m/sec*

Notes: Correlation with 3D simulations was done by considering V_r, W and P_{top} over all the storm cases given in Table 1 of Hueso and Sánchez-Lavega (2001). Values of P_{top} are rough estimates since dispersion of the data was very high. However, the correlation between W and V_r is much better. Remarks: (*) Updrafts of this magnitude can originate at the ammonia cloud level under certain conditions and require no water contribution to moist convection. (†) Updrafts require the condensation of water. A variety of water abundance may fit these values, for instance 0.2 solar composition and relative humidity ~99 % or 1 solar abundance of water in a drier humid environment with relative humidity ~75%. (§) This case is only possible under the most favorable environment conditions (water abundance ≥ 1 solar, 99 % relative humidity and full precipitation of condensed water).

Table 2

Summary of cluster model simulations

Run	**Grid characteristics**		**Storm elements**		**Results** (*t* = 120 *hrs*)	
	Grid points	ΔX	V_r	ΔC	N	V_{tang}
Nom	900 x 900	10 km	30 *m*/*s*	250 *km*	150	170
V1	800 x 800	"	15	250	195	70
V2	"	"	40	250	95	200
D1	"	"	30	100	900	90
D2	"	"	30	300	115	140

Notes: N is the number of single cells and V_{tan} in m/s is the tangential velocity in the system periphery.

Figure 1

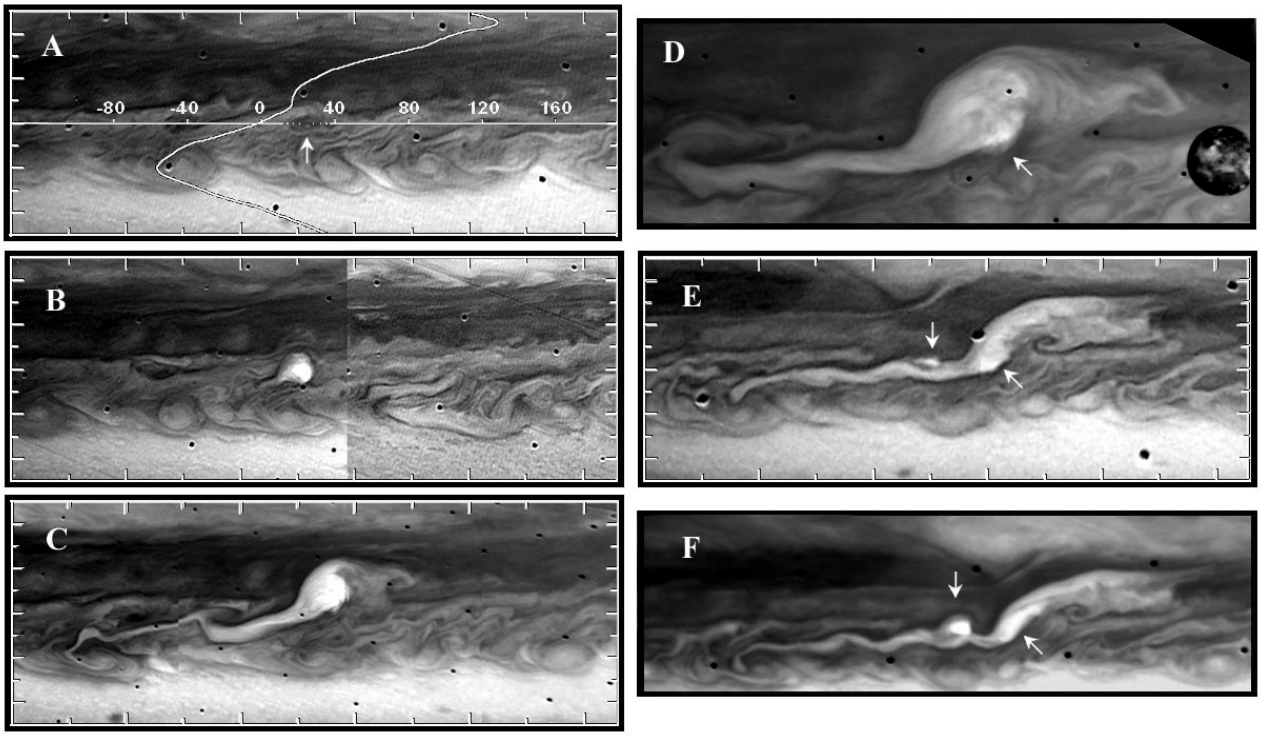

Figure 2

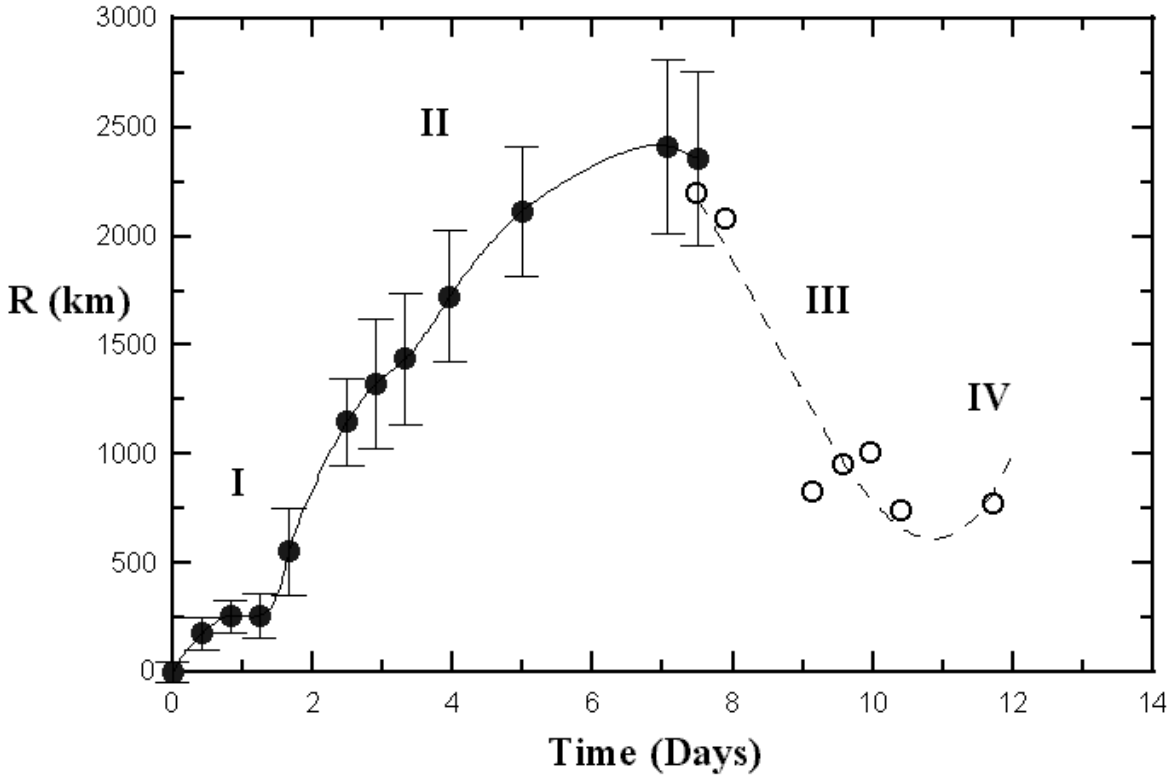
R (km)
Time (Days)
I
II
III
IV
0
500
1000
1500
2000
2500
3000
0
2
4
6
8
10
12
14

Figure 3

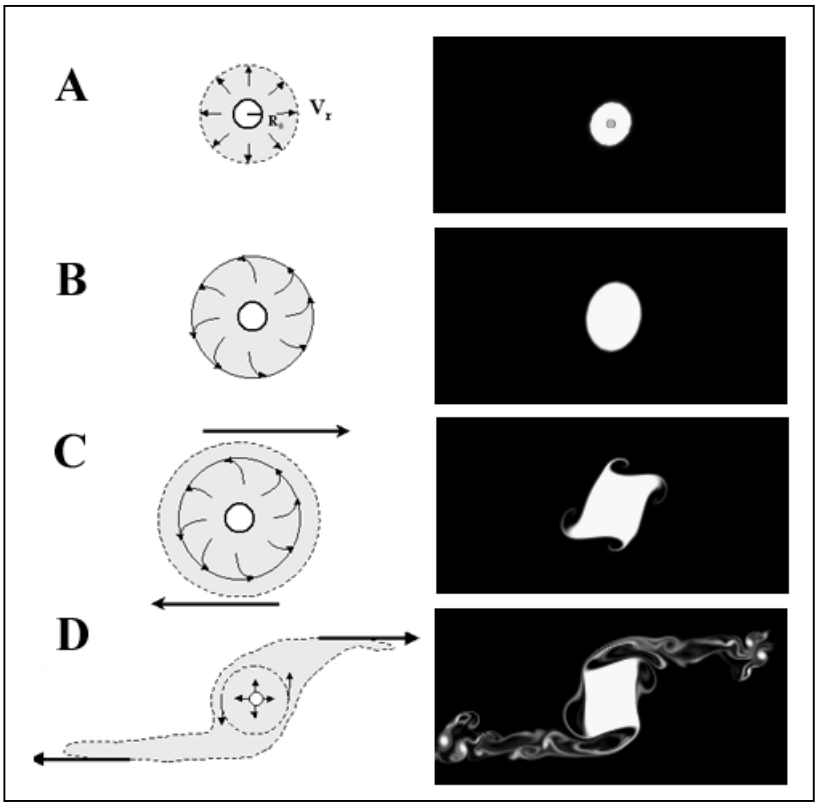

Figure 4

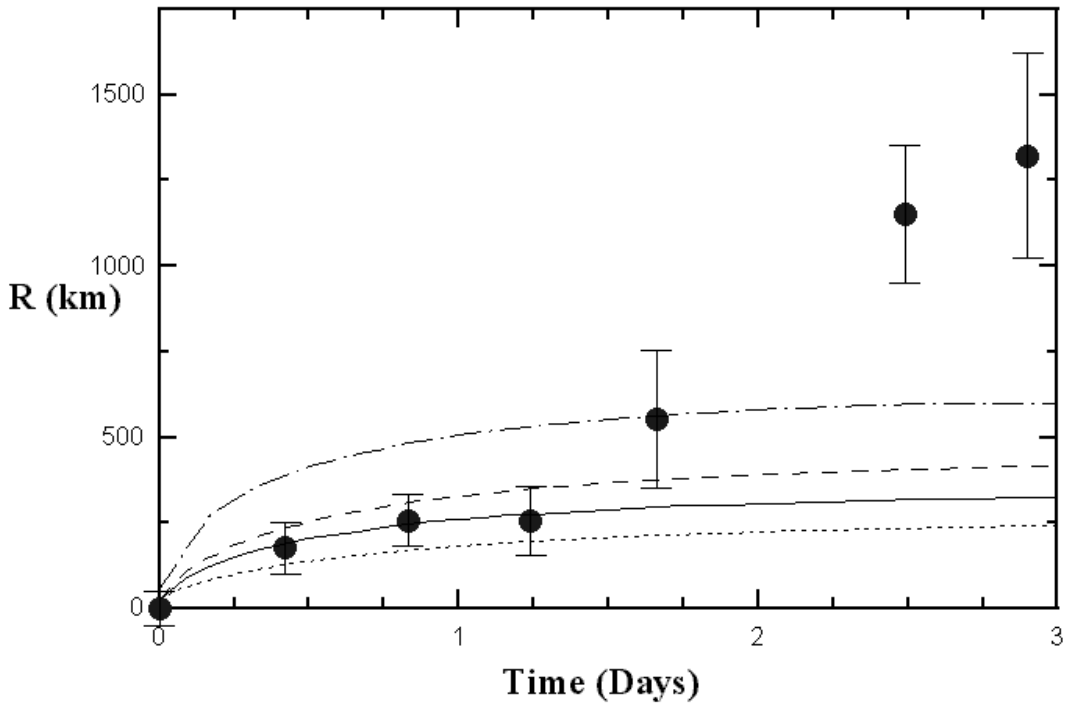

Figure 5

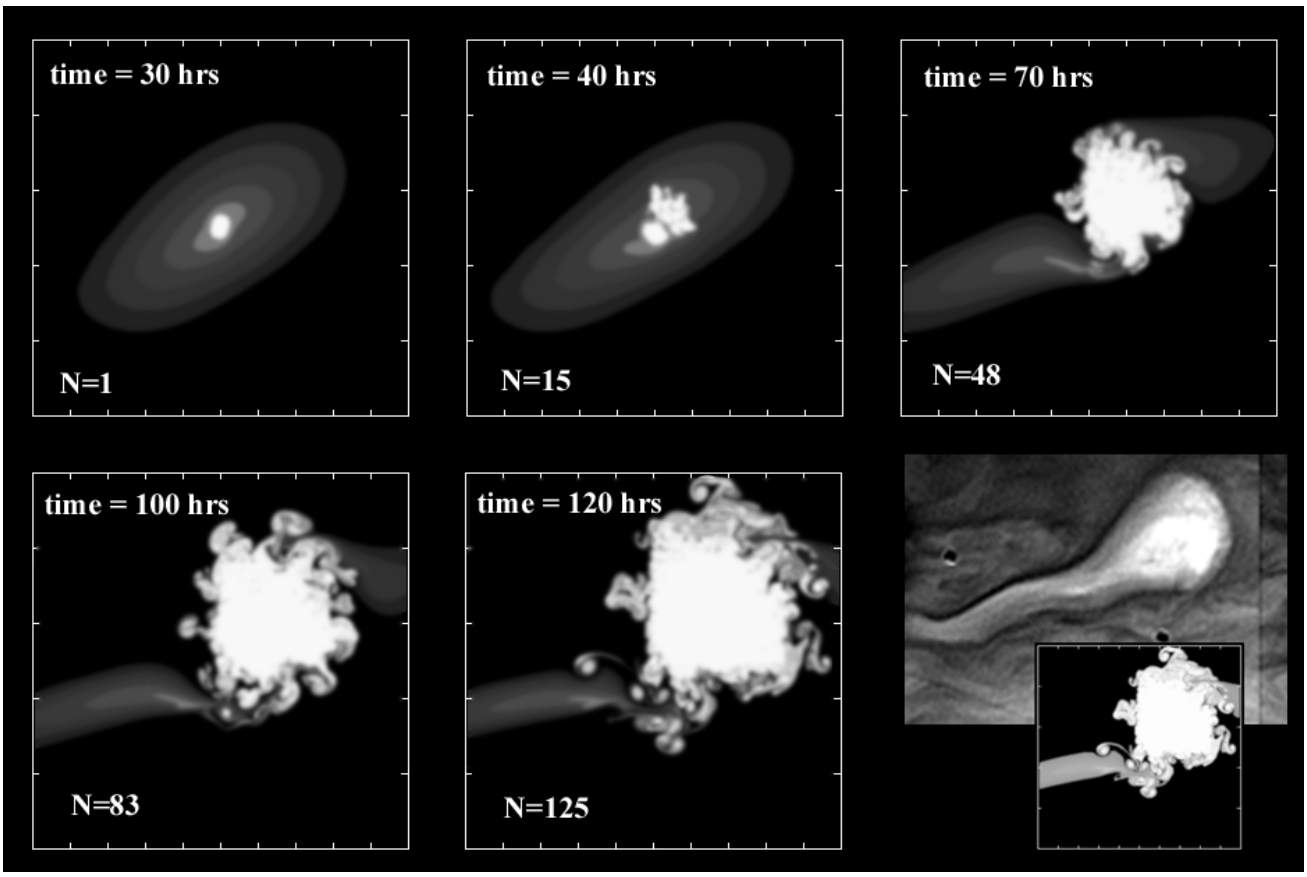
time = 30 hrs
N=1
time = 40 hrs
N=15
time = 70 hrs
N=48
time = 100 hrs
N=83
time = 120 hrs
N=125

Figure 6

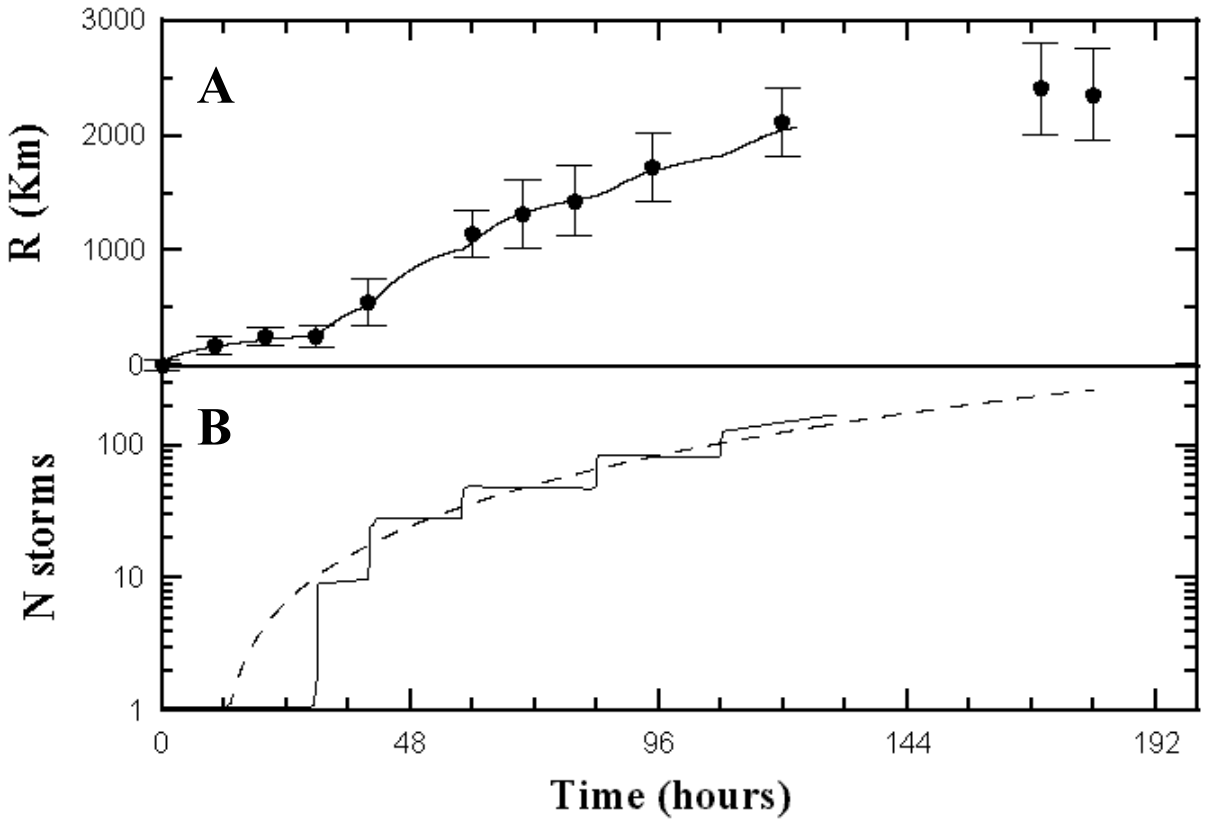
A
B
R (Km)
N storms
Time (hours)
3000
2000
1000
0
100
10
1
0
48
96
144
192

Figure 7

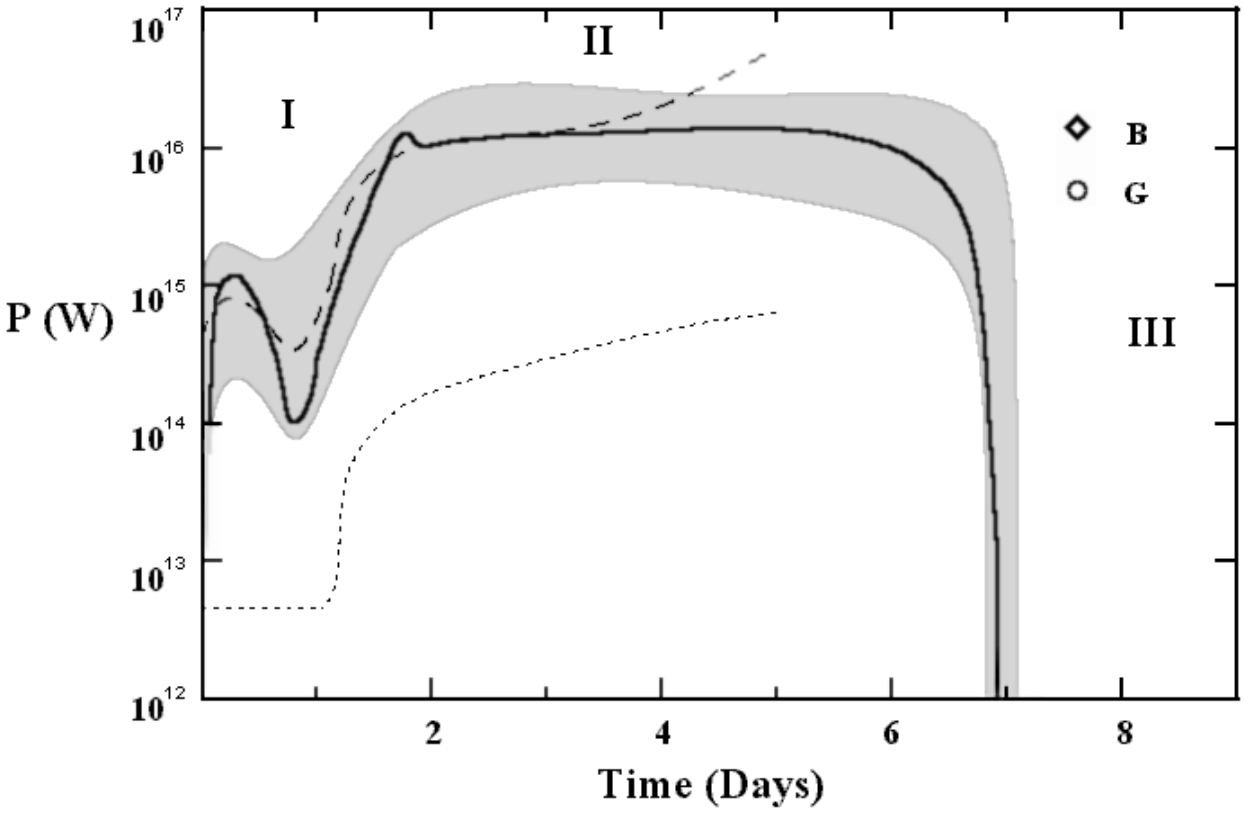

Figure 8